Journal of Petroleum
Science and Technology

Application of M^{3}GM in a Petroleum Reservoir Simulation

Ehsan Taheri [1]*, Amoirodin Sadrnejad[2], and Hasan Ghasemzadeh[2]

[1] Faculty of Engineering, Tarbiat Modares University, Tehran, Iran
[2] Faculty of Civil Engineering, K. N. Toosi University of Technology, Tehran, Iran

ABSTRACT

Reservoir formations exhibit a wide range of heterogeneity from micro to macro scales. A simulation that involves all of these data is highly time consuming or almost impossible; hence, a new method is needed to meet the computational cost. Moreover, the deformations of the reservoir are important not only to protect the uppermost equipment but also to simulate fluid pattern and petroleum production strategy. In this regard, multiscale multiphysic mixed geomechanical model (M^{3}GM) is recently developed. However, applications of petroleum reservoirs through gas or water injection in the depleted reservoir are in concern. In the present paper, a multiscale finite volume framework and a finite element method are employed to simulate fluid flow and rock deformation respectively. The interactions of solid and fluid phases are instated through the M^{3}GM framework. Then, its application in the petroleum reservoir through injection process is validated. The numerical results are compared with the fine scale simulations and reasonable agreement with high computational efficiency is obtained.

Keywords: Multiscale, Petroleum Reservoir, Computational Efficiency, Interaction, Injection

INTRODUCTION

Flow transport in petroleum reservoirs widely ranges from micro to macro scales. By considering these scales, interactions with solid phase make a great challenge in a petroleum reservoir simulation. In this regard, various upscaling and multiscaling models were developed in recent two decades [1-8]. However, all models are only in concern of fluid mechanics and geomechanical effects have been neglected [9,10]. It is worth mentioning that geomechanical effects are important not only to predict settlements in order to protect the uppermost facilities but also to simulate flow path and production strategy [10,11]. On the other hand, several geomechanical incidents such as surface subsidence which damages the uppermost installations, wellbore instability, and environmental issues have increased attention in this area [12-14]. In this regard, several models with different trends were developed to incorporate geomechanical effects [15-29]. Nevertheless, in all the models the fluid and solid scales are identical. However, every physic property has major effects on their domains of influence. Therefore, in order to place any event in the right position and save computational costs, it would be efficient to treat multiple physical

***Corresponding author**

Ehsan Taheri
Email: e_taheri@modares.ac.ir
Tel: +98 21 8288 4355
Fax: +98 21 8288 4324

Article history

Received: August 16, 2015
Received in revised form: April 23, 2016
Accepted: September 24, 2016
Available online: July 22, 2017

phenomena separately. In this context, recently, multiscale multiphysic mixed geomechanical model (M^3GM) is developed by the authors to simulate different physic through speared scales [9,10]. In the present paper, the fluid mechanic framework with multiscale finite Volume (MSFV) is described. Then, the finite element framework is employed to simulate geomechanical aspects. Moreover, the interaction between the fluid and solid phases is stablished through an appropriate algorithm. After the theoretical basis of the model is justified, its application to petroleum reservoirs, particularly to water injection in depleted petroleum reservoirs, is revealed

MULTISCALE WHY AND WHEN?

Several physical phenomena in the nature such as the mechanical behavior of composite materials and flow in porous media occur on a wide variety of physical scales from millimeter for pore scale to several kilometers with respect to reservoir dimensions [30,31]. The various scales of reservoir are shown in Figure 1. It should be mentioned that a conventional reservoir has computational modules in the order of 10^7-10^8 elements [32].

The number of elements could be increased with respect to the dimensions and complexity pattern of the geological formations. On the other hand, current computers are capable of simulating 10^5-10^6 elements [32]. In order to fill this gap, multiscale simulation is a crucial method [33-35]. Moreover, several physics, namely solid mechanics and fluid transport, are affected with respect to different orders of the influential domain [9,10,30]. In this regard, a framework which could simulate these wide ranges of scale lengths and physics is not available. Therefore, upscaling methods were developed, especially in the petroleum reservoir simulation [36-41]. Nevertheless, in upscaling methods, the reservoir problem have only been solved on a coarse scale, and the fine scale information have been lost [33,34]. On the contrary, in a multiscale framework, the fine scale properties are preserved during the homogenization and are used in resolution in the reference scale [33]. Thus, extensive motivations have been emerged into the multiscale modeling of the reservoir formation during 2003-2015 [9,10,42-54]. Figure 2 shows the methodology of upscale and multiscale methods to simulate reservoir formations [10].

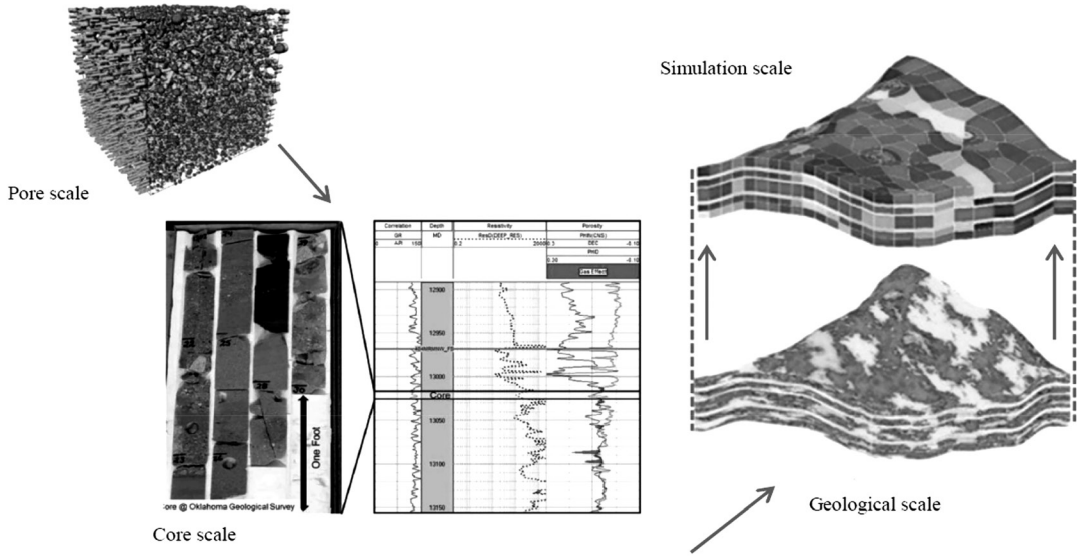

Figure 1: Indicative scales in petroleum reservoirs

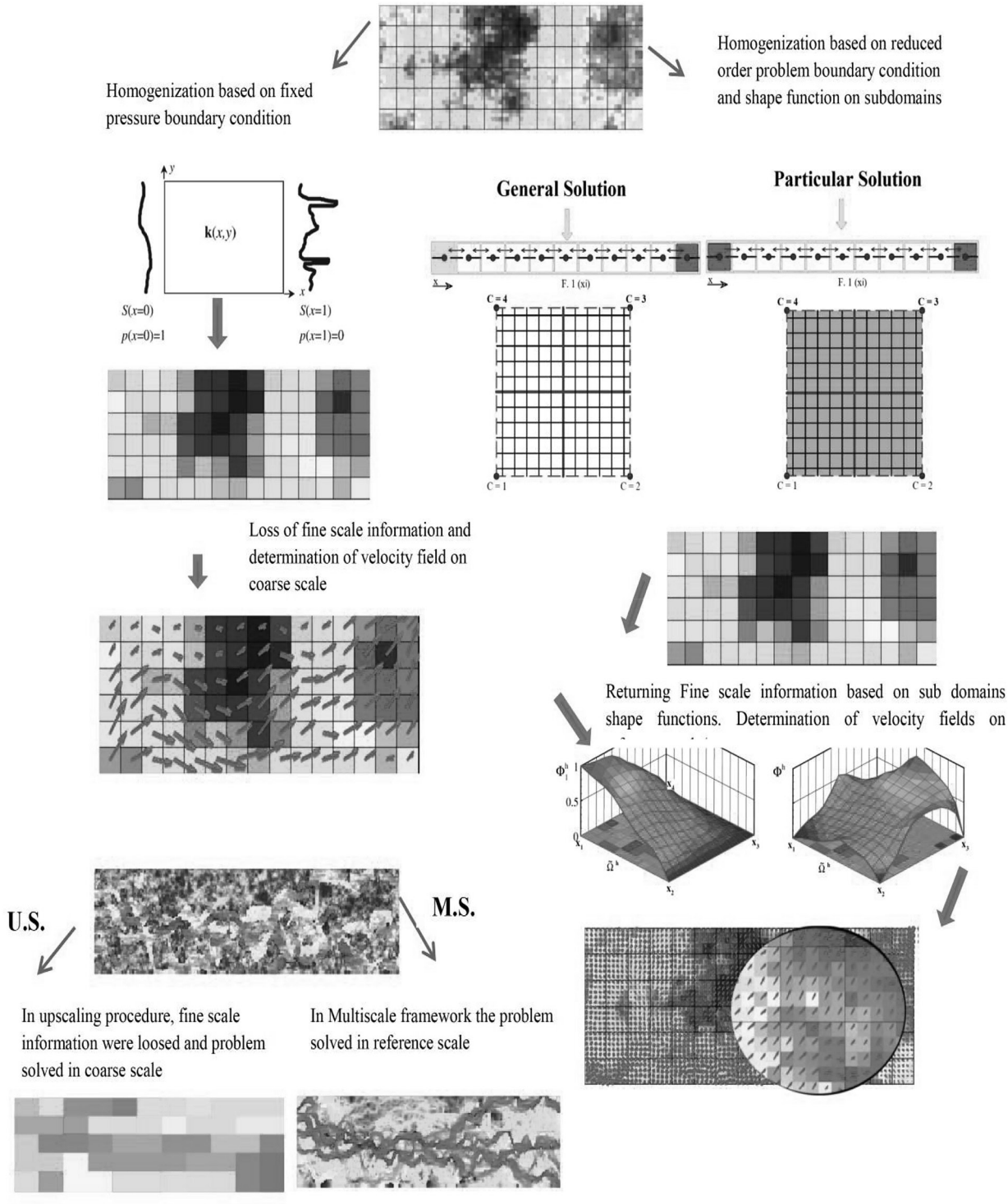

Figure 2: Comparison of upscale and multiscale procedures to simulate reservoir formation.

In the present paper, the MsFVM framework is applied with respect to preserving the fine scale specifications during upscaling and also mass conservative feature of the proposed method. The structure of the utilized Multi-scale method relies on separation of pressure and saturation equation the same as streamline method. However, with respect to limitation of streamline method for the depletion derive and deformable porous media [55&56], the adoptive updating of basis function regarding the saturation front is applied in order to solve saturation equation with high efficiency [10].

Governing Equations

In this section, in order to simulate fluid phases and porous media deformation and their interactions, the principle equations of mass and momentum of each phase are explained.

Fluid Phase

It is pointed out in the literature that fluid transport is in Eulerian, but soil transport is in Lagrangian point of view [11]. However, since there are both fluid and solid in the system, the fluid is observed from the deformed porous media not from a fixed mesh.

Mass Balance

The general mass conservation is governed by Equation 1:

$$\frac{dM}{dt}=\frac{d}{dt}\int_{V_t}\rho dV=0 \tag{1}$$

where, ρ is a phase density, and M stands for total mass. Moreover, with respect to Reynold theorem, one may obtain:

$$0=\frac{dM}{dt}=\int_{V_t}\frac{\partial\rho}{\partial t}dV+\int_{S_t}\rho\mathbf{v}.\mathbf{n}dS=0 \tag{2}$$

applying Gauss law will result in:

$$0=\frac{dM}{dt}=\int_{V_t}\left(\frac{\partial\rho}{\partial t}+\nabla.(\rho\mathbf{v})\right)dV \tag{3}$$

Thus by defining a relative velocity instead of interstitial velocity, by employing material derivatives, and by doing some mathematical manipulation, one may obtain:

$$\frac{D^s(\phi S_\alpha\rho_\alpha)}{Dt}+\nabla.(\phi S_\alpha\rho_\alpha\mathbf{w}_\alpha)+\phi S_\alpha\rho_\alpha\nabla.\mathbf{v}_s=\dot{m}_\alpha \tag{4}$$

where, ϕ is porosity, and S_α is phase saturation; $\mathbf{w}_\alpha$ represents relative velocity. Also, $\mathbf{w}_\alpha=\mathbf{v}_\alpha-\mathbf{v}_s$; $\mathbf{v}_\alpha$ is velocity, and $\mathbf{v}_s$ is solid skeleton velocity; $\dot{m}_\alpha$ stands for sink or source term. Since the system of concern is made up of two fluid phases, two mass balances, i.e. Equation 4, are taken into account.

Momentum Balance of Fluid Phase

In order to simulate fluid flow and set up interaction between phases, momentum balance should be considered.

$$\varphi_\alpha S_\alpha W_\alpha=\lambda_\alpha.(-\nabla p+\rho_\alpha\,\mathbf{g}) \tag{5}$$

where, λ_α is phase mobility tensor defined as $\lambda_\alpha=\frac{Kkr_\alpha}{\mu_\alpha}$ and **K** represents the inherent permeability tensor; Kr_α stands for relative permeability and is simulated as a function of the pertinent phase saturation, and μ_α is the phase viscosity.

Solid Phase

With respect to history conservation aspect [11], the solid deformation is considered in Lagrangian point of view.

Mass Balance of Solid Phase

The solid phase mass balance is stated as follows:

$$\frac{\partial}{\partial t}(1-\varphi)\rho_s+\nabla.(1-\varphi)\rho_s\mathbf{v}_s=0 \tag{6}$$

Neglecting grain compressibility leads to:

$$\frac{\partial(1-\varphi)}{\partial t}+\mathbf{v}_s.\nabla(1-\varphi)+(1-\varphi)\nabla.\mathbf{v}_s=0 \tag{7}$$

$$\varepsilon_{vol}=\nabla.\mathbf{u}_s \tag{8}$$

Finally, utilizing material derivative and the mechanical definition of deformation rate will lead to:

$$\frac{-1}{1-\varphi}\frac{D(1-\varphi)}{Dt}=\frac{D\varepsilon_{vol}}{Dt} \tag{9}$$

Equation 9 will also be used to state the interaction between solid and fluid phases.

Momentum Balance of Solid Phase

The momentum balance of the solid phase is governed by the following equation:

$$\nabla.\boldsymbol{\sigma}+\rho\mathbf{g}=0 \tag{10}$$

where, σ is total stress tensor. However, in geomechanical considerations, the effective stress σ' is applied instead.

$$\sigma' = \sigma - \mathbf{I} p_t \tag{11}$$

where, P_t is pore fluid pressure.

Multiscale Multiphysic Fluid and Solid Interaction

The interactions of the solid and fluid phases are stated through a Newton-Raphson iteration loop with respect to solid deformation and fluid phase pressure. Furthermore, by integrating Equation 9, one may obtain:

$$\varphi = (1-(1-\varphi_0)\exp[-\varepsilon_{vol}]) \tag{12}$$

As stated in Equation 12, porosity will change with respect to the stress evolution and the related volumetric strain. In general, phase mobility is related to porosity through chain rule derivatives. However, in order to keep the basic functions (which will be defined later) off the iteration loop, the explicitly incorporation of porosity changes is take into account.

Multiscale Multiphysic Geomechanical Model (M³GM)

M³GM is established by coupling the fluid phases transport and solid skeleton deformation as explained below.

Multiscale Finite Element Framework

By incorporating the momentum balance of solid and fluid phases in Equation 4, by the implicit time discretization of the resulted formula, and by integrating over all phases (for detailed mathematical information, interested readers are referred to our previous researches [9,10]) one may obtain:

$$\frac{\varphi^{n+1}}{\Delta t} + \frac{-\varphi^n}{\Delta t}\sum_{\alpha=1}^{n_p} B_\alpha^{n+1}\rho_\alpha^n S_\alpha^n - \sum_{\alpha=1}^{n_p} B_\alpha^{n+1}\nabla.(\rho_\alpha^{n+1}\boldsymbol{\lambda}_\alpha(\nabla p^{n+1} - \rho_\alpha^{n+1}\mathbf{g}\nabla z)) + \varphi^{n+1}\frac{\varepsilon_v^{n+1}-\varepsilon_v^n}{\Delta t} = q_t \tag{13}$$

where, n and $n+1$ are two sequential time steps, and B_α is a formation volume factor defined as the inverse of phase density.

The superposition of basis and correction functions (general and specific solutions of homogenous and inhomogeneous parts of Equation 4 with respect to the reduced problem boundary conditions) will lead to:

$$p_f(x) \approx p'(x) = \sum_{h=1}^{N}\left[\sum_{k=1}^{M}\Phi_k^h(x)\bar{p}_k + \Phi^h(x)\right] \tag{14}$$

By integration over all coarse cells, one may obtain:

$$\int_{\bar{\Omega}_l}\frac{C_c}{\Delta t}\left(\sum_{h=1}^{N}\left(\sum_{k=1}^{M}\Phi_k^h\bar{p}_k^{v+1} + \Phi^{h^v}\right) - p^{'v}\right)d\Omega - \int_{\partial\bar{\Omega}_l}\left(\boldsymbol{\lambda}_t.\sum_{h=1}^{N}\left(\sum_{k=1}^{M}\Phi_k^h\bar{p}_k^{v+1} + \Phi^{h^v}\right)\right).\tilde{\mathbf{n}}_l d\Gamma = \int_{\bar{\Omega}_l} RHS^v d\Omega \tag{15}$$

which will form the system of equation:

$$\mathbf{A}_{lk}\mathbf{p}_k^{v+1} = \mathbf{b}_l^v \tag{16}$$

where,

$$\mathbf{A}_{lk} = \sum_{h=1}^{N}\left(\int_{\bar{\Omega}}\frac{C_c}{\Delta t}\Phi_k^h d\Omega - \int_{\partial\bar{\Omega}_l}(\boldsymbol{\lambda}_t.\nabla\Phi_k^h).\tilde{\mathbf{n}}_l d\Gamma\right) \tag{17}$$

and

$$\mathbf{b}_l^v = \int_{\bar{\Omega}}\left(RHS^v + \frac{C_c}{\Delta t}p^{'v}\right)d\Omega - \sum_{h=1}^{N}\left(\int_{\bar{\Omega}}\frac{C_c}{\Delta t}\Phi^{h^v}d\Omega - \int_{\partial\bar{\Omega}}\boldsymbol{\lambda}_t.\nabla\Phi^{h^v}.\tilde{\mathbf{n}}_l d\Gamma\right) \tag{18}$$

The above nonlinear system of equations will be sequentially solved until convergence is achieved.

Finite Element Framework

As mentioned earlier, the finite element method is employed for solid deformation framework. Eight node of a serendipity family shape function is applied in this regard (see Figure 3).

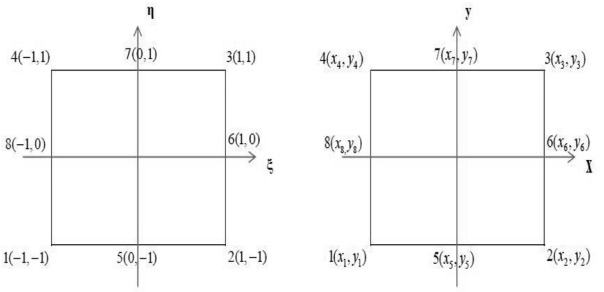

Figure 3: A solid phase element with a serendipity 2D family shape function.

The classical finite element weighted residual discretization of Equation 11 leads to:

$$\int_{\Omega} \mathbf{W}_u^t (\mathbf{L}^T \sigma - \rho \mathbf{g}) d\Omega + \int_{\Gamma_u} \overline{\mathbf{W}}_u^t (\mathbf{L}^T \sigma - \overline{\mathbf{t}}) d\Gamma = 0 \quad (19)$$

By implementing Gauss theorem and stress-strain relation, one may obtain (interested readers are referred to our previous works [9, 10]):

$$\left[\int_{\Omega} \mathbf{B}^T \mathbf{D} \mathbf{B} \quad d\Omega\right] \hat{\mathbf{u}} = -\int_{\Gamma^N} \mathbf{N}_u^T \overline{t} d\Gamma + \int_{\Omega} \mathbf{B}^T (p\mathbf{m}) d\Omega \quad (20)$$

which results in a linear deformation system:

$$\mathbf{K}\hat{\mathbf{u}} = \mathbf{F} \quad (21)$$

where:

$$\mathbf{K} = \left[\int_{\Omega} \mathbf{B}^T \mathbf{D} \mathbf{B} \quad d\Omega\right] \quad (22)$$

and

$$\mathbf{F} = -\int_{\Gamma^N} \mathbf{N}_u^T \overline{t} d\Gamma + \int_{\Omega} \mathbf{B}^T (p\mathbf{m}) d\Omega = \mathbf{F}_1 + \mathbf{F}_2 \quad (23)$$

The first term in the right hand side of Equation 22 is obtained from the finite element boundary condition. However, the second term is achieved with respect to the integration over the fine pressure attained from the multiscale framework.

$$\mathbf{F}_2 = \sum_{i=1}^{i=nfs} B_i^T p_i .m.A \quad (24)$$

NUMERICAL RESULTS

Water Injection in Homogeneous Rigid Media

The first test is water injection in homogenous reservoirs with the inherent permeability of $2.5\times10^{-13}m^2$. The viscosity ratio is 5, and the reservoir is initially filled with oil. In order to verify the model, the results are compared with the simulation of White and Lewis in 1991 [55]. The Brook & Corey's relative permeability function is selected to compare the results. In addition, a quadratic function is also utilized to evaluate the relative permeability constitutive function. As it is clear from Figure 4, although fine scale is employed, the contour is deviated from a quarter circle shape which is expected. In order to modify the results, Geiger and coworkers simulate the case by combining finite element and finite volume methods [56]. The results with 4096 elements are also shown in Figure 4. As it is clear from Figure 4, reasonable agreement is observed with just 100 elements in new multiscale methods. It should be noted that, in petroleum reservoir development, lots of scenarios are performed to allocate the most appropriate situation for injection. In this regard, the computational efficiency of the multiscale models is the crucial matter.

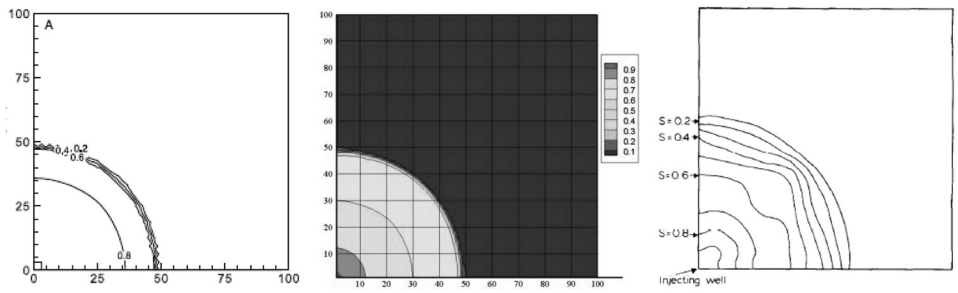

Figure 4: Saturation contours: left: finite element after White & Lewis; middle: after Geiger et al.; right: M³GM.

Moreover, in order to precisely evaluate model accuracy, pressure and saturation contours at three points, namely A (3, 3), B (1, 11), and C (14, 14), are compared with a fine scale. As shown in Figures 5 and 6, the trend and the amount of results are in rational agreement. The pressure at point A (the point closer to injection well) is reduced sharply with respect to a rapid flow front, while at points B and C, the pressure drops smoothly since injection fluid front reaches this area. As shown in Figure 6, the oil saturation curves also follow the same path. It is apparent from Figure 5 that the quadratic constitutive relation of relative permeability with saturation fails to predict the pressure fall correctly. Although the pressure curves have little discrepancies, the saturation curves are fitted closely. It shows that little deviation in the calculation of saturation will lead to more errors in the pressure estimation.

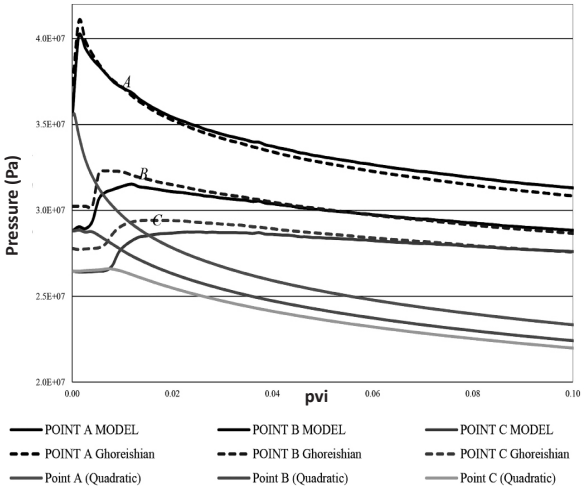

Figure 5: Pressure history curves at pints A, B, and C from fine scale and M^{3}GM simulations.

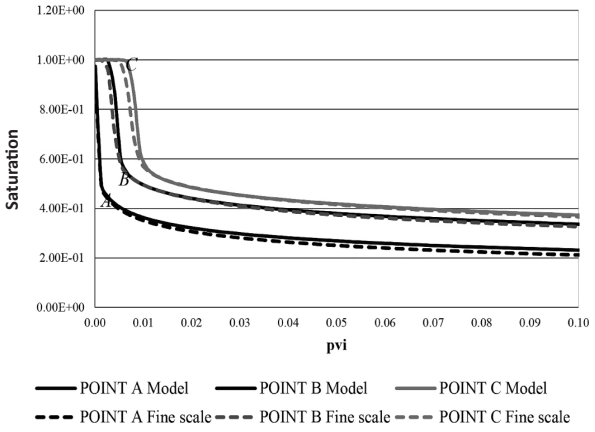

Figure 6: Comparison of oil saturation history curves at points A, B, and C of fine scale and M^{3}GM simulations.

Water Injection in Heterogeneous Deformable Porous Media

In order to evaluate the effect of mesh construction in a multiscale model, water injection in heterogeneous porous media is presented. The permeability field belongs to Tarbert formation and is a part of 20th layer of SPE 10 [40] as shown in Figure 7. The size of the problem was selected in a way to evaluate four different mesh sizes, namely (15×15-3×3), (9×9-5×5), (5×5-3×3), and (3×3-15×15). The first set of numbers are related to the numbers of coarse cells in each direction, and the second set shows the number of fine cells encapsulated in each spatial direction of a coarse cell. The porous media is initially filled with 85% oil and 15% water. The initial pressure is 10 kPa. In order to increase the pressure, water is injected in the lower left corner, i.e. fine cell (1, 1), and production occurs from the upper right corner, i.e. fine cell (54, 54) at a constant pressure. The oil in place has a viscosity value 4 times more than that of the injected water. The pressure and saturation contours are depicted in Figure 8 after 0.11 PVI. As it is clear from this figure, the injected water front follows the lower permeability field and deviates from the quarter circle shape in a homogenous permeability pattern, which was reported in a homogenous case. However, in

order to evaluate the effect of coarse grid construction and related mesh, the pressure values at three locations of the domain with coordinates of A (2, 2), B (12, 16), and C (4, 28) are assessed.

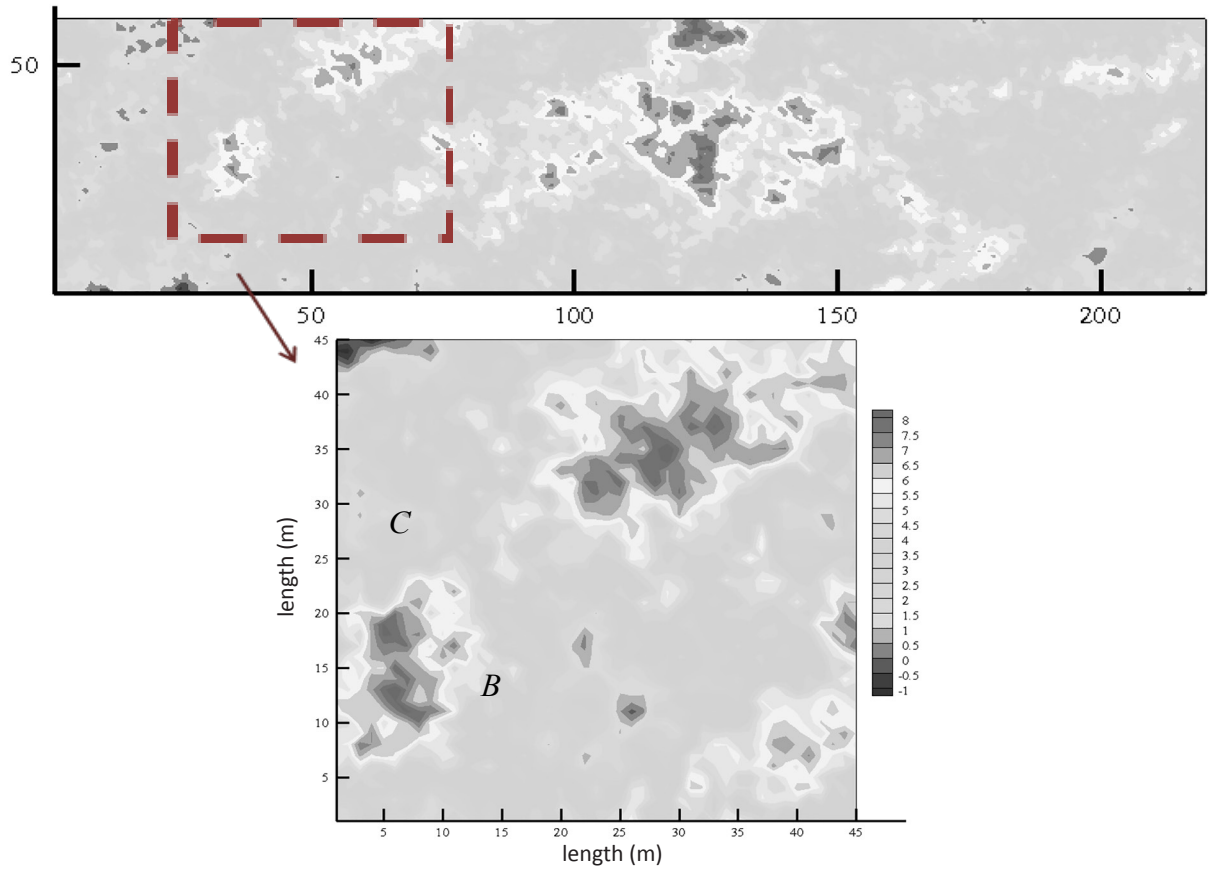

Figure 7: Permeability field belonging to Tarbert formation is obtained from 20th layer of SPE 10.

The pressure values at these locations are compared with the four sets of meshes of those locations mentioned earlier.

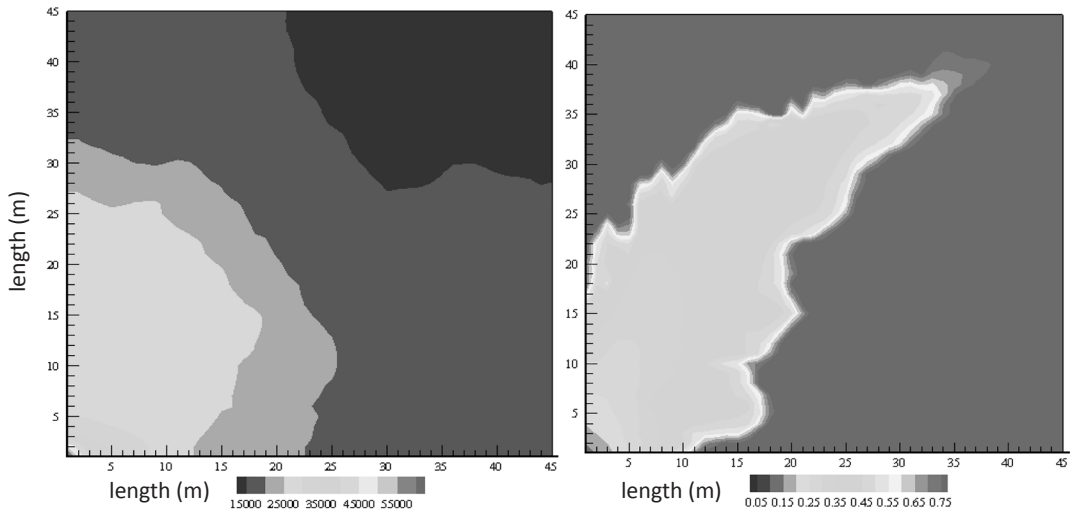

All Dimension are in meter.

Figure 8: Pressure and oil saturation contours after 0.11 PVI.

As shown in Figure 9, reasonable agreement is observed in mesh (15×15-3×3), (9×9-5×5), and (5×5-3×3). However, in a coarser cell, i.e. (3×3-15×15), the result oscillates and do not converge, which is due to the fact that the flow front fills just one coarse cell and affects the hardness matrix. Also, considering high contrast permeability value in the construction of coarse grid and avoiding constructing a dual cell border in this region are recommended.

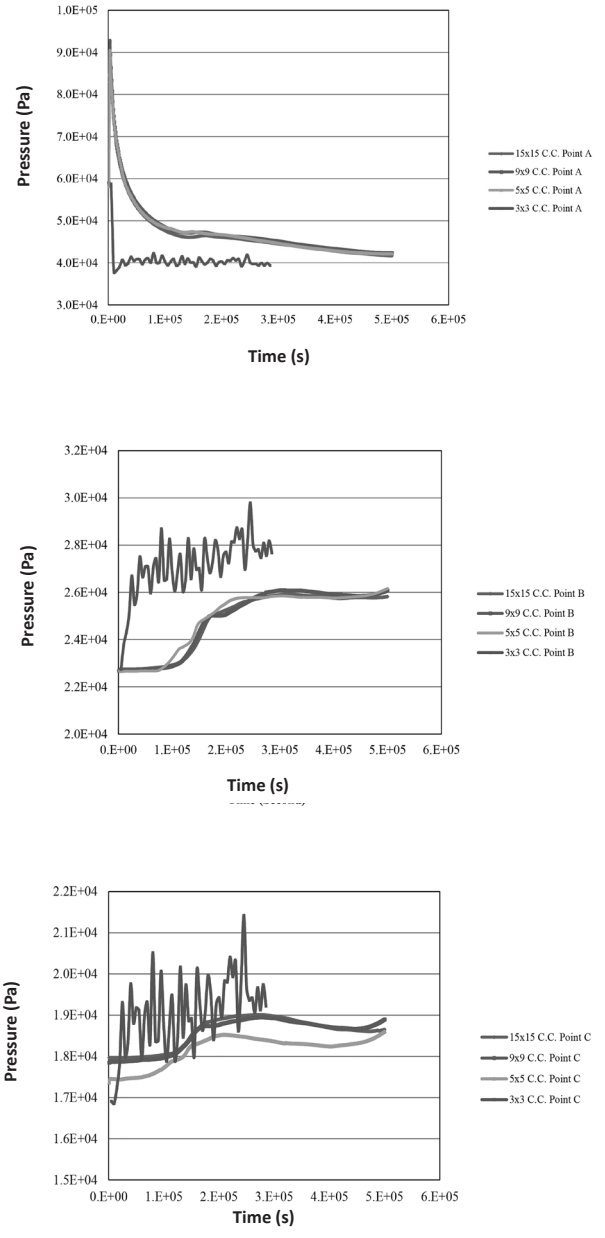

Figure 9: Pressure history at points A, B, and C through different mesh sizes.

On the other hand, the deformations of reservoir formation are important not only to preserve the uppermost facilities, but also to predict fluid flow and production rare correctly. Figure 10 shows the deformation of the reservoir domain through water injection. The elastic modules and Poisson's ratio are considered 25 MPa and 0.25 respectively. The mechanical boundary conditions and mesh sizes are also shown in Figure 10. As it is clear from this figure, the maximum deformations take place on the top of the injection well, where the maximum pressure changes are observed.

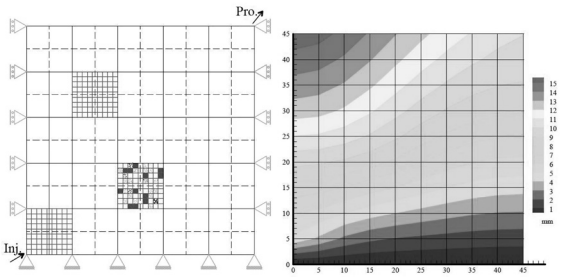

Figure 10: Left: A schematic of water injection and mechanical boundary conditions' right: the deformation distribution of the soil domain in a five-spot water flood problem after 0.085 PVI.

Moreover, production rate through injection is shown in Figure 11 in fine scale and multiscale frameworks. As shown in this figure, the multiscale results are in good agreement with the fine scale solution.

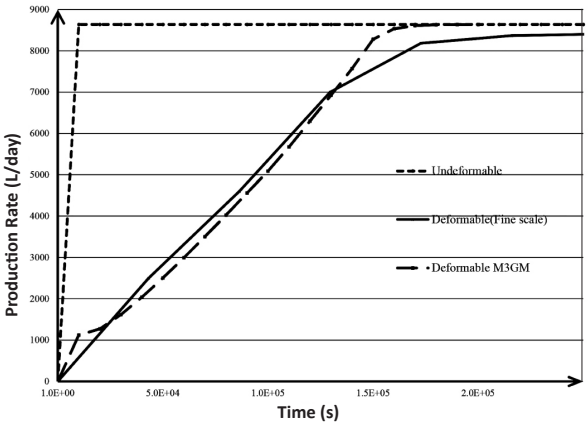

Figure 11: Production rate in a five-spot problem within the reservoir in the rigid and deformable media.

It worth mention that in Multiscale frame work 81 coarse element is utilize in compare with 2025 fine scale model and 25 times savings is obtained. Moreover, as it is clear from Fig. 11 the production rate in the porous media with consideration of deformation is lower than in rigid media that is more realistic. Since in the real field the reservoir formations are not rigid, some energy of injection is consumed through the deformation of rock media. While the injection proceeds, the deformations of rock media have been occurred and productions rate is asymptotes to the threshold value. As explained heretofore, the validity and efficiency of the model are confirmed with respect to aforementioned test cases. However, the robustness of the model will be shown by the highly heterogeneous layer of Tarbert formation by the full domain of 20th layer of SPE 10 as shown in Fig. 7. This layer has the mean and variance of the natural logarithm mean and variance of 2.35 and 5.66, respectively. The permeability varies over 6 orders of magnitude. The injection is imposed by the 10 times less viscos fluid from the fine cell (1,1) and the production with constant pressure of 0 at fine cell (220, 55).

No-flow boundary conditions are considered at the domain borders. The physical properties of fluids and mechanical parameters of porous media are shown in Table. 1. Fine scale results are obtained from Hajibeygi (2011). In the present Multiscale model, two different scales (coarse and fine) for the pressure deformation and saturation equation are applied respectively. The M3GM utilize 20 × 5 coarse grid and 220 × 55 fine grid cells, with respect to pressure deformation and saturation field resolution, respectively. The pressure field and saturation font contours are shown in Fig. 12 After 0.132 PVI.

Table 1: Physical properties of fluids and mechanical parameters of porous media.

μ_o	μ_w	ρ_o	ρ_w	ϕ	S_o	Δx	Δy	E	υ
$10^{-2}\,Pa.s$	$10^{-3}\,Pa.s$	$950\frac{kg}{m^3}$	$1000\frac{kg}{m^3}$	0.2	1	1m	1m	350 *kPa*	0.2

As it is clear from Fig. 11, M3GM results are in the same pattern as the fine scale solution. Figure 13 also shows the deformation of the formation after 0.132 PVI. The maximum deformations take place above the injection well where the pressure and effective stress changes is on the peak.

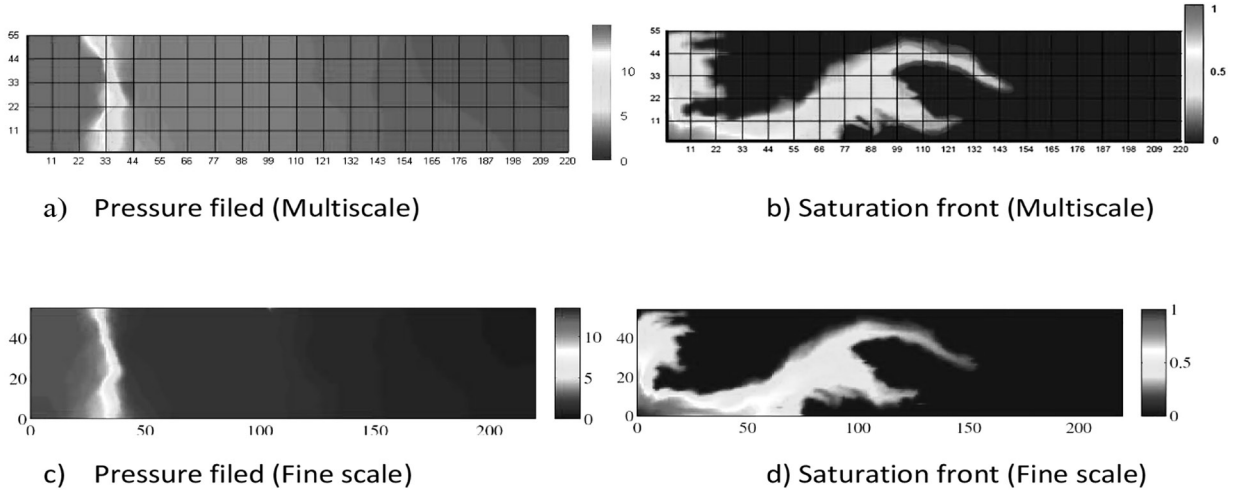

Figure 12: comparison of pressure filed saturation front between M3GM and fine scale solution after 0.132 PVI

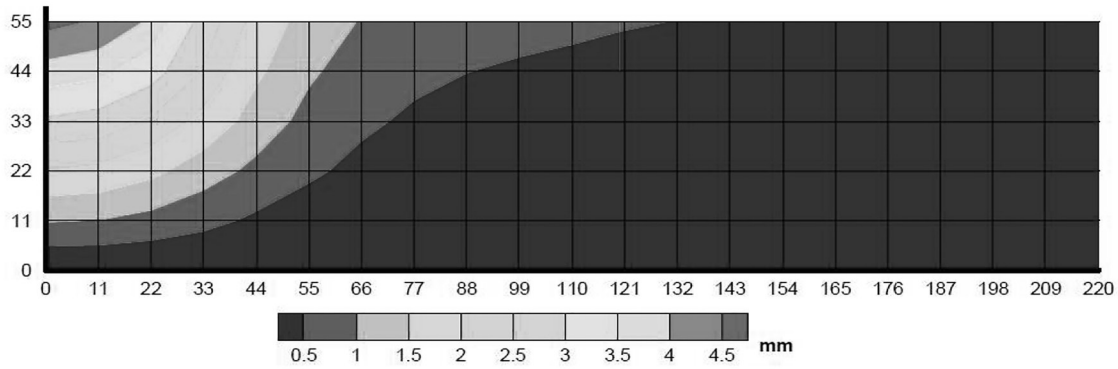

Figure 13: M3GM deformation fields of SPE 10 Tarbert formation after 0.132 PVI

It is important that during injection and depletion, deformation of reservoir also could have undesirable effects on the sensitive uppermost facilities with respect to settlement or heave. In this regard, instrumentations such as shut down valves, High-integrity pressure protection system (HIPPS), mechanical equipment such as floating storage tank that are easily affected by deformation and other deformation sensitive equipment should be located with reliable distance from this region especially in onshore area.

CONCLUSIONS

The new model namely, M³GM, is presented by considering the multiscale and multiphysic nature of reservoir porous media. Its application in the petroleum reservoir through water injection in depleted reservoirs is validated. The M³GM model confirms the results of other methods at high computational efficiency. The present model not only simulates fluid flow in porous media, but also evaluates the deformation of the reservoir domain.

REFERENCES

1. Aarnes J. E., "On the Use of a Mixed Multiscale Finite Element Method for Greater Flexibility and Increased Speed or Improved Accuracy in Reservoir Simulation," *Multiscale Model Simul*., **2004**, *2*, 421-439.
2. Arbogast T., "Implementation of a Locally Conservative Numerical Sub-grid Upscaling Scheme for Two-phase Darcy Flow," *Comput. Geosci.*, **2002**, *6*, 453-481.
3. Durlofsky L. J., "Numerical Calculation of Equivalent Grid Block Permeability Tensors for Heterogeneous Porous Media," *Water Resource Research*, **1991**, *27*, 699-708.
4. Durlofsky L. J., "Upscaling of Geocellular Models for Reservoir Flow Simulation: A Review of Recent Progress," *International Forum on Reservoir Simulation. Buhl/Baden-Baden*, Germany, **2003**, 1-58.
5. Farmer C. L., "Upscaling: A review," *Int. J. Numer. Meth Fluids*, **2002**, *40*, 63-78.
6. Chen Z. and Hou T. Y., "A mixed multiscale finite element method for elliptic problems with oscillating coefficients," *Math. Comput*., **2002**, *72*, 541–576.
7. Efendiev Y., Ginting V., Hou T. Y., and Ewing R.,

"Accurate Multiscale Finite Element Methods for Two-phase Flow Simulations," *J. Comp. Phys*., **2006**, *220*, 155–174.

8. Hajibeygi H. and Jenny P., "Multiscale Finite-volume Method for Parabolic Problems Arising from Compressible Multiphase Flow in Porous Media," *Computational Physics*, **2009**, *228*, 5129-5147.
9. Sadrnejad S. A., Ghasemzadeh H., and Taheri E., "Multiscale Multiphysic Mixed Geomechanical Model in Deformable Porous Media," *Journal for Multiscale Computational Engineering*, **2014**, *12*(6), 529-547.
10. Taheri E., "Multiscale Modeling of Oil Transport in Deformable Porous Media," Ph.D. Thesis, K. N. Toosi University of Technology, **2015**.
11. Lewis R. W. and Schrefler B. A., "Finite Element Method in the Static and Dynamics Deformation and Consolidation of Porous Media," (2nd Ed.) England, Wiley, **1998.**
12. Bruno M. S. "Subsidence-induced Well Failure," In SPE (Chevron Oil Field Research, Society of Petroleum Engineers), SPE 20058-PA, **1992**.
13. Rhett D. W. and Revisited E., "A New Model of Ekofisk Reservoir Geomechanical Behavior," In SPE/ISRM Rock Mechanics in Petroleum Engineering, (Trondheim, Norway 1998), **1990**.
14. Carbognin L., Gatto P., Mozzi G., and Gambolati G., "Land subsidence of Ravenna and its similarities with the Venice case. Proceedings of the Engineering Foundation Conference on Evaluation and Prediction of Subsidence," New York: ASCE, **1978**, 254-266.
15. Lewis R. W. and Sukirman Y., "Finite Element Modelling for Simulating the Surface Subsidence above a Compacting Hydrocarbon Reservoir," *Int. J. Analytic. Numer. Meth. Geomech.*, **1993**, *18*, 619-639.
16. Li X. and Zienkiewicz O. C., "Multiphase Flow in Deforming Porous Media and Finite Element Solutions," *Computers & Structures*, **1992**, *45*(2), 211-227.
17. Minkoff S. E., Stone C. M., Bryant S., Peszynska M., et al., "Coupled Fluid Flow and Geomechanical Deformation Modeling," *Journal of Petroleum Science and Engineering*, **2003,** *38*, 37-56.
18. Phillips P. J. and Wheeler M. F. "A Coupling of Mixed and Continuous Galerkin Finite Element Methods for Poroelasticity I: the Continuous in Time Case," *Comput. Geosci.*, **2007**, *11*, 131-144.
19. Phillips P. J. and Wheeler M. F., "A Coupling of Mixed and Continuous Galerkin Finite Element Methods for Poroelasticity II: The Discrete-in-time Case," *Comput. Geosci.*, **2007**, *11*, 145-158.
20. Settari A. and Walters D. A., "Advances in Coupled Geomechanical and Reservoir Modeling With Applications to Reservoir Compaction," SPE Reservoir Simulation Symposium, Houston, Texas, **1999**.
21. Settari A. and Mourits F. M., "Coupling of Geomechanics and Reservoir Simulation Models. Proc. Of the 8th Int. Conf. on Computer Methods and Advances in Geomechanics," Morgantown, West Virginia, **1994**, 2097-2158.
22. Dean R. H., Gai X., Stone C. M., and Minkoff S. E., "A Comparison of Techniques for Coupling Porous Flow and Geomechanics," In SPE Reservoir Simulation Symposium (Houston 2003), SPE 79709, **2003**.
23. Gutierrez M. and Lewis R. W. "The Role of Geomechanics in Reservoir Smulation," In Proceedings of the SPE/ISRME; ROCK198, (SPE paper 47392) (Trondheim, Norway, **1998**.
24. Gutierrez M., Lewis R. W., and Masters I. "Petroleum Reservoir Simulation Coupling Fluid

and Geomechanics," SPE Reservoir Evaluation & Engineering, **2001**, *4*, 164-171.

25. Wan J., Durlofsky L. J., Hughes T. J. R., and Aziz K. "Stabilized Finite Element Methods for Coupled Geomechanics Reservoir Flow simulations," In SPE Res Simul Sym (SPE 79694) (Houston 2003).
26. Jeannin L., Mainguy M., Masson R., and Gilbert S. V. "Accelerating the Convergence of Coupled Geomechanical-reservoir Simulations," *Int. J. Numer. Anal. Meth. Geomech*., **2007**, *31*, 1163–1181.
27. Prevost J. H. "Partitioned Solution Procedure for Simultaneous Integration of Coupled-field Problems," *Commun. Numer. Meth. Engng.*, **1997**, *13*, 239-247.
28. Wheeler M. F. and Gai X., "Iteratively Coupled Mixed and Galerkin Finite Element Methods for Poroelasticity," *Numer Meth for PDEs*, **2007**, *23*, 785–797.
29. Kim J., Tchelepi H. A., and Juanes R., "Rigorous Coupling of Geomechanics and Multiphase Flow with Strong Capillarity," *SPE Journal*, **2013**, 1123-1139.
30. Aarnes J. E., Kippe V., Lie K. A., and Rustad A. B. "Modelling of Multiscale Structures in Flow Simulations for Petroleum Reservoirs in Geometrical Modeling," *Numerical Simulation and Optimization Applied Mathematics at SINTEF. Springer*, Verlag, **2007**.
31. Sadrnejad S. A., Ghasemzadeh H., and Taheri E., "Multiscale Advance Features in Modeling Oil Transport in Porous Media," In 21st Annual International Conference on Mechanical Engineering-ISME, Tehran, Iran, **2013**.
32. Wen X. H., Durlofsky L. J., and Edwards M. G., "Use of Border Regions for Improved Permeability Upscaling," *Mathematical Geology*, **2003**, *35*, 521-547.
33. Jenny P., Lee S. H., and Tchelepi H. A., "Multi-scale Finite-volume Method for Elliptic Problems in Subsurface Flow Simulation," *Computational Physics*, **2003**, *187*, 47-67.
34. Jenny P., Lee S. H., and Tchelepi H. A. "Adaptive Fully Implicit Multi-scale Finite-volume Method for Multi-phase Flow and Transport in Heterogeneous Porous Media," *Journal of Computational Physics*, **2006**, *217*, 627-641.
35. Lee S. H., Wolfsteiner C., and Tchelep H. A., "Multiscale Finite-volume Formulation for Multiphase Flow in Porous Media: Black Oil Formulation of Compressible, Three-phase Flow with Gravity," *Computational Geoscience*, **2008**, *12*, 351-366.
36. King M. J., MacDonald D. G., Todd S. P., and Leung, H., "Application of Novel Upscaling Approaches to the Magnus and Andrew Reservoirs," SPE European Petroleum Conference. The Hague, The Netherlands, SPE 50643, **1998**.
37. Chen Y., Durlofsky L. J., Gerritsen M., and Wen X. H., "A Coupled Local–global Upscaling Approach for Simulating Flow in Highly Heterogeneous Formations," *Advances in Water Resources*, **2003**, *26*, 1041-1060.
38. Wen X. H., Durlofsky L. J., and Edwards M. G., "Upscaling of Channel Systems in Two Dimensions Using Flow-based Grids," *Transport in Porous Media*, **2003**, *51*, 343–366.
39. Peszy´nska M., Wheeler M. F., and Yotov I., "Mortar upscaling for multiphase flow in porous media," *Comput. Geosci*., **2002**, *6*, 73-100.
40. Christie M. and Blunt M. , "Tenth SPE Comparative Solution Project: a Comparison of Upscaling Techniques," *SPE Reserv. Evaluat. Eng*., **2001**, *4*, 308–317.
41. Durlofsky L. J. "Upscaling of Geocellular Models for Reservoir Flow Simulation: A Review of Recent

Progress," In International Forum on Reservoir Simulation (Buhl/Baden-Baden), Germany, **2003**, 1-58.

42. Jenny P., Lee S. H., and Tchelepi. H. A., "Adaptive Multiscale Finite-Volume Method For Multiphase Flow And Transport In Porous Media," *Multiscale Model. Simul*., **2004**, *3*, 50-64.
43. Lee S. H., Wolfsteiner C., and Tchelep H. A., "Multiscale Finite-volume Formulation for Multiphase Flow in Porous Media: Black Oil Formulation of Compressible, Three-phase Flow with Gravity," *Computational Geoscience*, **2008**, *12*, 351-366.
44. Jenny P. and Lunati I. "Modeling Complex Wells with the Multi-scale Finite-volume Method," *Journal of Computational Physics*, **2009**, *228*, 687–702.
45. Lee S. H., Zhou H., and Tchelepi H. A. "Adaptive Multiscale Finite-volume Method for Nonlinear Multiphase Transport in Heterogeneous Formations," *Journal of Computational Physics*, **2009**, *228*, 9036–9058.
46. Lunati I. and Jenny P., "Multiscale Finite-volume Method for Density-driven Flow in Porous Media," *Computational Geoscience*, **2008**, *12*, 337-350.
47. Hajibeygi H., Bonfigli G., Hesse M. A., and Jenny P., "Iterative Multiscale Finite-volume Method," *Journal of Computational Physic*, **2008**, *227*, 8604–8621.
48. Hajibeygi H. and Jenny P. "Adaptive Iterative Multiscale Fnite Volume Method," *J. Comput. Phys*., **2011**, *230*, 628–643.
49. Aarnes J. E. and Efendiev Y. "Mixed Multiscale Finite Element for Stochastic Porous Media Flows," *SIAM Sci. Comp.*, **2008**, *30*, 2319–2339.
50. Efendiev Y., Ginting V., Hou T. Y., and Ewing R. "Accurate Multiscale Finite Element Methods for Two-phase Flow Simulations," *J. Comp. Phys*., **2006**, *220*, 155–174.
51. Efendiev Y., Hou T. Y., and Wu X. H., "Convergence of a Nonconforming Multiscale Finite Element Method," *SIAM J. Numer. Anal*., **2000**, *37*, 888–910.
52. Hou T. Y., Wu X. H., and Cai Z. "Convergence of a Multiscale Finite Element Method for Elliptic Problems With Rapidly Oscillating Coefficients," *Math. Comput*., **1999**, *68*, 913–943.
53. Efendiev Y. and Hou T. Y. "Multiscale Finite Element Methods Theory and Applications," Series: Surveys and Tutorials in the Applied Mathematical Sciences, Springer, **2009**.
54. Lunati I. and Jenny P., "Treating Highly Anisotropic Subsurface Flow With The Multiscale Finite-Volume Method," *Multiscale Model. Simul*., **2007**, *6*, 308-318.
55. Samier P., Quettier L., and Thiele M. "Applications of Streamline Simulations to Reservoir Studies," *SPE Res. Eval. & Eng.*, SPE-78883-PA, **2002**, *5*(4): 324–332.
56. Baker R. O., Kuppe F., and Chug S., et al., "Full-Field Modeling Using Streamline-Based Simulation: 4 Case Studies," Presented at *the SPE Reservoir Simulation Symposium*, SPE-66405-MS, Houston, Texas, **2001**.
57. White I. R. and Lewis R. W., "The Numerical Simulation of Multiphase Flow Through a Porous Medium and its Application to Reservoir Engineering," *Applied Mathematical Modelling*, **1981**, *5*(3), 165–172.
58. Geiger S., Roberts S., Mattha S. K., Zoppou C., et al., "Combining Finite Element and Finite Volume Methods for Efficient Multiphase Flow Simulations in Highly Heterogeneous and Structurally Complex Geologic Media," *Geofluids*, **2004**, *4*, 284–299.